A New Methodology to Assess Building Integrated Roof Top Photovoltaic Installations at City Scales: The Tropical Coastal City Case

Rabindra Pokhrel[1]
Department of Mechanical Engineering,
The City College of New York,
New York, NY 10031
e-mail: rpokhre000@citymail.cuny.edu

Andy Walker
Energy Systems Integration Directorate,
National Renewable Energy Laboratory (NREL),
Golden, CO 80401
e-mail: andy.walker@nrel.gov

Jorge E. González
Department of Mechanical Engineering,
NOAA-CREST Center,
The City College of New York,
New York, NY 10031
e-mail: jgonzalezcruz@ccny.cuny.edu

As a consequence of the warm and humid climate of tropical coastal regions, there is high energy demand year-round due to air conditioning to maintain indoor comfort levels. Past and current practices are focused on mitigating peak cooling demands by improving heat balances by using efficient building envelope technologies, passive systems, and demand side management strategies. In this study, we explore city-scale solar photovoltaic (PV) planning integrating information on climate, building parameters and energy models, and electrical system performance, with added benefits for the tropical coastal city of San Juan, Puerto Rico. Energy balance on normal roof, flush-mounted PV roof, and tilted PV roof are used to determine PV power generation, air, and roof surface temperatures. To scale up the application to the whole city, we use the urbanized version of the Weather Research and Forecast (WRF) model with the building effect parameterization (BEP) and the building energy model (BEM). The city topology is represented by the World Urban Database Access Portal Tool (WUDAPT), local climate zones (LCZs) for urban landscapes. The modeled peak roof temperature is maximum for normal roof conditions and minimum when inclined PV is installed on a roof. These trends are followed by the building air conditioning (AC) demand from urbanized WRF, maximum for normal roof and minimum for inclined roof-mounted PV. The net result is a reduced daytime Urban Heat Island (UHI) for horizontal and inclined PV roof and increased nighttime UHI for the horizontal PV roof as compared with the normal roof. The ratio between coincident AC demand and PV production for the entire metropolitan region is further analyzed reaching 20% for compact low rise and open low rise buildings due to adequate roof area but reaches almost 100% for compact high rise and compact midrise buildings class, respectively.
[DOI: 10.1115/1.4045347]

Keywords: air conditioning, building, cooling, energy, integrated systems, smart buildings, solar, sustainability

1 Introduction

Due to concerns on environmental pollution on a global and societal level, there has been an urge to shift the fossil fuel and nuclear energy generation to reliable and sustainable energy sources installed at the location of the load. Among all the renewable energy sources, solar energy is one of the most abundant and the cleanest energy source [1]. To support the shift to sustainable generation, integrated urban and energy planning on every aspect of the energy demand and integration of different systems has to be considered [2]. In addition to integrated planning, a recent study highlights that the built environment of the future would transform buildings into resource assets-fully self-aware, adaptive and communicative with added market value [3]. Present and future buildings: residential, commercial, or industrial sectors can have additional value if utilized through generation at specific location and space. Direct solar energy conversion stemming from roof areas will play a significant role in the context of sustainable generation by a mix of renewable energies [4]. As an example, the relevance of the large availability of roof surface area for some northern cities of Spain was found to have relatively high potential for solar PV despite lower irradiance [5]. For other locations, it has been estimated that the application of solar PV technology can provide about two-thirds of the current electricity consumption in the city of Bardejov in eastern Slovakia [6] with a population of 33,000. As an additional example, the modern residential district of Scharnhauser Park near Stuttgart/Germany, with a population of 7000 people, was used to calculate the potential of photovoltaic (PV) energy and to evaluate the ratio of "own consumption" defined as the ratio of total electricity consumption by the energy produced. Ratio of own consumption of 17% was estimated with the total yearly electricity consumption of 10,700 MW h [7]. The electricity potential generated from the rooftop solar PV system in the Gangnam district in Seoul, South Korea, can be enough to supply 303,496 households (3724.5 kW h/year/household), almost 1.5 times more than the households in the district (202,906 households) [8].

To determine the PV potential of larger spaces, tools have also been developed to estimate the energy production and cost of energy of grid-connected photovoltaic applications around the world, e.g., PV Watts developed by the U.S. National Renewable Energy Laboratory (NREL[2]) as a good example. However, these tools are single building or site specific and do not consider urban effects for large city applications. It is therefore important to

[1]Corresponding author.
Manuscript received April 22, 2019; final manuscript received September 23, 2019; published online October 30, 2019. Assoc. Editor: Shiguang Miao.

[2]https://pvwatts.nrel.gov

incorporate urban morphology to consider the urban heterogeneity that includes the radiation trapping and shadowing due to building heights. Also, the role of PV installation on meeting and mitigating energy demands, mitigating Urban Heat Islands (UHIs), and consequently air pollution on a city-scale are important considerations to take into account. We find that integration into the larger built environment and the larger utility system is just as important as other drivers such as solar resource and cost to the use of PV to achieve energy sustainability and resilience goals. In hot, humid climates, the coincidence of cooling load with solar resource provides a valuable opportunity for such integration of supply with demand.

Energy demand can be influenced by socioeconomic factors; however, air conditioning (AC) demand is amplified in very warm climates in the tropics or during extreme heat conditions in temperate climates and here we seek to mitigate this demand in order to reduce the stress on the electric grid and facilitate increasing amounts of PV generation. The U.S. Department of Energy (DOE) reports that energy consumption by heating ventilation and air conditioning (HVAC) accounts for 63% and 36.7% of the total electrical energy use for residential and commercial buildings, respectively [9]. For the entire world, the building energy consumption by HVAC in 2010 was 61% for residential and 40% for commercial buildings [10]. Further, the energy consumption by HVAC has been increasing due to economic growth and global climate change. It has been estimated that energy demand for cooling would increase by 15% over the 21st century [11], and summer loads would increase by 10% for most U.S. buildings [12]. AC demands peak during an extreme heat wave day and increases by 20% as compared with a normal day [13]. For the specific context of tropical coastal locations, the extreme heat events were studied for the Mesoamerican and Caribbean (MAC) region defined as three consecutive days with daily maximum heat index greater than the 97th percentile of the datasets [14,15]. In the same study, it was reported that 144 extreme heat wave events were recorded for entire Mesoamerican and Caribbean region out of which 11 events were recorded for the city San Juan, Puerto Rico for a period of 35 years (1980–2014) [14]. During an extreme heat event, a high-pressure atmospheric system induced southeasterly winds (as opposed to normal easterly winds) was responsible for the recorded high summer temperatures, leading to high rates of mortality related to heat stroke and cardiovascular diseases as reported for San Juan during the summer of 2012 [16]. Also, the projection of the number of heat wave events per year was estimated to be between 12 and 15 for the future climate period of 2026–2045 for Puerto Rico [15]. Heat waves in general would be occurring with a higher frequency and intensity in the future, resulting in risks to the population and without air conditioning systems maybe at higher health risks under these conditions. For the MAC region, a research agenda is proposed in order to better understand and inform on appropriate mitigation and adaptation efforts as a consequence of extreme events, to secure local infrastructure and health of community residents [17]. It thus becomes important to quantify energy demand requirements to maintain human comfort level during these very warm conditions in tropical coastal regions and to apply best mitigating strategies to reduce the overall and peak cooling demands. Here, we explore different active (building integrated PV systems) and passive (cool roof (CR)) technologies in order to mitigate peak demands with its added benefits of power production at a city scale.

At least 40 GW of PV systems were installed globally in 2014, up from 37 GW in 2013 setting a new record for the solar PV sector. China, Japan, and USA were the three top markets in 2014. The 540 GW mark at a global level could be reached in 5 years' time (by 2019) [18]. The large sector of PV installation is seen in utility-scale PV installation, accounting 57.0% and building-scale PV accounting for 42% of the total market share in China [19]. As building-scale PV is gaining popularity because of the availability of roof space and utility-cost savings, the importance of geo-spatial information and 3D information, which could be unique for each city, becomes necessary for the estimation of PV potential for sites within urban areas. A recent development in the estimation of PV potential in urban areas uses CityGML,[3] which describes 3D city and landscape model including geometry, semantic, topology, and appearance. This model has been improved to include PV simulations including shading of buildings in urban settings [7]. However, the interaction between the urban climate and the buildings as well as determining the ratio of demand to production becomes essential for every urban environment and it is missing from current analysis tools. To account for the interaction between climate, buildings, and energy demand with PV mounted roof, the use of non-hydrostatic version of the Weather Research and Forecast (WRF). WRF [20] coupled to the multilayer building energy (BEP + BEM) system [21] has been recently conducted for the cities of Tucson and Phoenix in Arizona [22]. The results demonstrate that the deployment of cool roofs and rooftop solar photovoltaic panels reduce near-surface air temperature and cooling energy demand at the scale of the metropolitan area. The parameterization adopted here, to characterize solar photovoltaic arrays in the multilayer BEM [22], is based on the scheme proposed by Masson et al. [23] and assumes horizontal PV mounted roof with reparameterizing of BEM including the balancing of sensible heat flux through roof. However, the methodology proposed in the present work considers horizontal PV roof (HPV) as well as tilted rooftop PV and cool roof, modifying the roof surface temperature as a consequence of the energy balance on roof under different conditions. This study focuses on roof surface temperature for different roof applications reporting on 2 m air temperature, AC demands, and solar power production.

Different roofing properties and technologies influence roof surface temperatures, which in turn affects the surface heat flux to the built environment. As an example, the roof surface temperature in Miami, FL is reported to reach 60 °C, 30 °C greater than air temperature, for roof surface albedo of 0.3 [24]. Thus, the use of different roof surface applications for city-scale deployment are effective means of reducing air temperature and energy consumptions [22,24–28]. For tropical conditions or summer seasons, cool roofs, by virtue of increased roof albedo, absorb less incoming shortwave radiation than dark roofs, thereby promoting a lower roof temperature. As a result, cool roofs reduce heat transfer into the urban environment and into the buildings, simultaneously decreasing near-surface air temperature and cooling energy demands. It has been recently reported that the cool roofs (albedo 0.85) and green roofs reduce the roof surface temperature by almost 8–10 °C [29]. Short-term simulation shows that the urban area is more efficient in partitioning surface energy balance when green roofs are specified as opposed to including vegetation inside the urban core [30]. However, the net positive effect of green roofs still unknown as some recent reports indicate that large-scale use has adverse impacts on the air quality due to changes in the atmospheric stability [31]. On the other hand, large-scale PV installations (on ground) have been shown to increase UHI effects significantly, especially during nights for all four seasons [32]; however, the effect on rooftop PV has been shown to decrease the temperature and UHI effects [22,23]. However, for the South Coast Air Basin of California, it was reported that rooftop PV have a net positive effect on the thermal storage of the buildings, an effect enhancing the existing UHI by up to 0.2 °C [33]. On building level studies carried for the city of San Diego, CA, maximum roof temperature reached 60 °C for normal roof (NR) (albedo 0.25) and 40 °C for tilted rooftop PV with a cooling load reductions potential of 4.8 W/m^2 (clear days) to 1.6 W/m^2 (under cloudy days) [34]. The observations and the simulations showed that the air quality became worse after the wind strength weakened and its direction disturbed due to strong UHI; these are conditions that led a convergence zone persisting over an urbanized area caused very high concentrations of pollutants, thereby affecting hospital respiratory admissions counts

[3]https://www.opengeospatial.org/standards/citygml

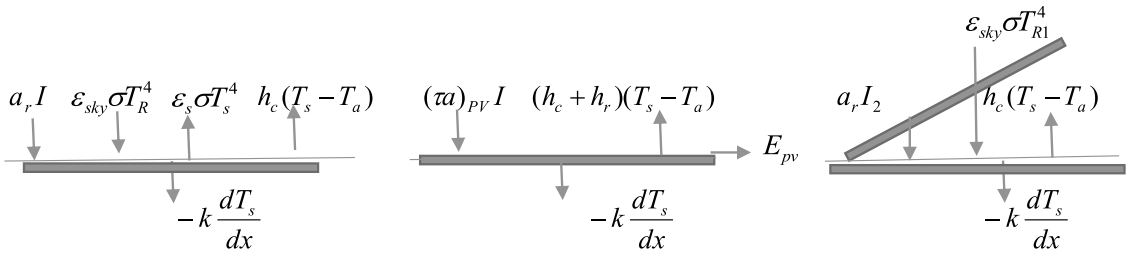

Fig. 1 Surface energy balance for normal roof, horizontal PV roof, and tilted PV roof

[35,36] and higher risk of human morbidity [37,38] due to heat stroke. Documented examples of the relations between discomfort index based on poor air quality and UHIs were reported for several locations. In Dali district of Taiwan, it was found that high UHI worsens the air quality, thus significantly increasing hospital admissions [36]. In other studies, it was determined that compact cities amplify the overall human discomfort by amplified UHI placing the population at higher risk [39]. For the costal tropical city of San Juan, Puerto Rico, it was recently reported that at an increase in UHI by 1 °C increases the Human discomfort index by 5% [40]. In the context of the coastal tropical cities such as those in the Caribbean, relevant science questions are *how do the regional warming climate and the local urbanization effects interact?; how do these interactions change with different building roofing technologies as mitigation options? and what may be the impacts of these two variables in social value variables such as energy and human comfort?* The first question has been addressed by other researchers such as Comarazamy et al. [41] and Velazquez-Lozada et al. [42], reporting that urbanization has a larger effect in the maximum surface temperatures while a changing regional climate in the hydrological cycles. This study will focus on the second and third question and study the comprehensive effect on 2 m air temperature, UHI, energy demands, and PV power potential as mitigation option for urban settings of tropical coastal environments, an important consideration to capitalize on environmental and energy sustainability stemming from roof areas.

As a case study, this study considers the San Juan Metropolitan Area (SJMA) of the Island of Puerto Rico, as a representative of tropical coastal urban environments. SJMA has a population of over 1.25 million containing nearly one-third of the overall population of the Island of Puerto Rico. The total coverage area for the city is 575 km^2 and electrical energy per capita is 282 kW h/year. The case study of the city of San Juan, Puerto Rico is considered due to the potential of this city to undergo rapid changes as part of the transformation post Hurricane Maria.[4] According to Puerto Rico Integrated Resource Plan 2018–2019 report, the renewable and alternative sources needs to increase by 20% by 2035 [43].

We thus investigate environmental and energy sustainability of urban coastal tropical city utilizing different roofing technologies. The changes in roof surface temperature for normal roof, horizontal PV roof, tilted PV roof, and cool roof are utilized to investigate 2-m air and roof temperatures along with energy demands. The radiation parameters are further utilized to study the potential of PV power output.

The structure of this contribution is as follows. Section 2 presents the methods used describing the proposed energy balance for normal flat roof, horizontal PV on the roof, and tilted rooftop PV. Section 3 elaborates the results and highlights different cooling load reduction potential for different roof applications, along with PV power potential. Section 4 summarizes the main conclusions and future works.

[4]The Puerto Rico state legislature adopted a bill that would set a 100% renewable portfolio standard (RPS) by 2050 as part of a broader package of energy reforms (https://www.utilitydive.com/news/puerto-rico-passes-100-renewable-energy-bill-as-it-aims-for-storm-resilien/551303/)

2 Methods

Energy balance is carried out for normal roof (Eq. (1)), horizontal PV roof (Eq. (10)), and tilted PV roof (Eq. (12)). These conditions are schematically represented in Figs. 1 and 2. For normal roof, the heat flux from the roof surface is balanced by the incoming solar radiation both shortwave and longwave and heat transfer by convection from the roof surface. The computed sol–air temperature (Eq. (5)) of the normal roof is a function of albedo (α), incoming solar radiation (I), the heat transfer coefficient (h_c and h_r), the ambient temperature (T_a), and the radiant temperature of sky (T_R). The roof surface temperature is computed from sol–air temperature by utilizing Eq. (17).

The surface energy balance of a horizontal PV roof is given by Eq. (10), where E_{pv} is the power produced by PV panel. The temperature of PV panel is assumed to be the surface temperature of the horizontal PV roof given by Eq. (11). The sol–air temperature in this case is dependent on ambient temperature and solar radiation, which is converted to surface temperature utilizing Eq. (17).

Finally, the surface energy balance of the tilted PV roof assumes that the radiation from the back of the PV panel is absorbed by the roof along with the incoming longwave radiation from the sky which is balanced by the outgoing radiation and convective heat flux from the surface of tilted PV roof. The sol–air temperature in this case is dependent on PV temperature, air temperature, the heat transfer coefficients, and surface albedo. Each of the parameters in the equations is defined in the nomenclature section. The following equations are per unit collector area (m^2) and per unit time (s).

Surface energy balance over flat (normal) roof

$$a_r I + \varepsilon_{\text{sky}}\sigma T_R^4 - \varepsilon_s\sigma T_s^4 - h_c(T_s - T_a) = -k\frac{\mathrm{d}T_s}{\mathrm{d}x} \tag{1}$$

$$h_r = \varepsilon\sigma(T_s + T_R)(T_s^2 + T_R^2) \cong 0.4h_c \text{ when } I > 0$$
$$\cong 0.3h_c \text{ when } I < 0 \tag{2}$$

$$h_c = 4U_a + 5.6 \tag{3}$$

$$T_R = 1.2T_a - 14$$

$$-k\frac{\mathrm{d}T}{\mathrm{d}x} = (h_c + h_r)(T_s' - T_s) \tag{4}$$

where T_s'= sol–air temperature [44,45].

From Eqs. (1)–(4), the surface temperature of normal roof is

$$T_s' = T_a + \frac{\alpha_r I}{h_0} - \frac{h_r}{h_0}(14 - 0.2T_a) \tag{5}$$

Energy balance over PV

$$(\tau a)_{PV} I = E_{pv} + U_{PV}(T_{PV} - T_a) \tag{6}$$

$$E_{PV} = [\varepsilon_R - \mu(T_{PV} - T_{\text{ref}})]I \tag{7}$$

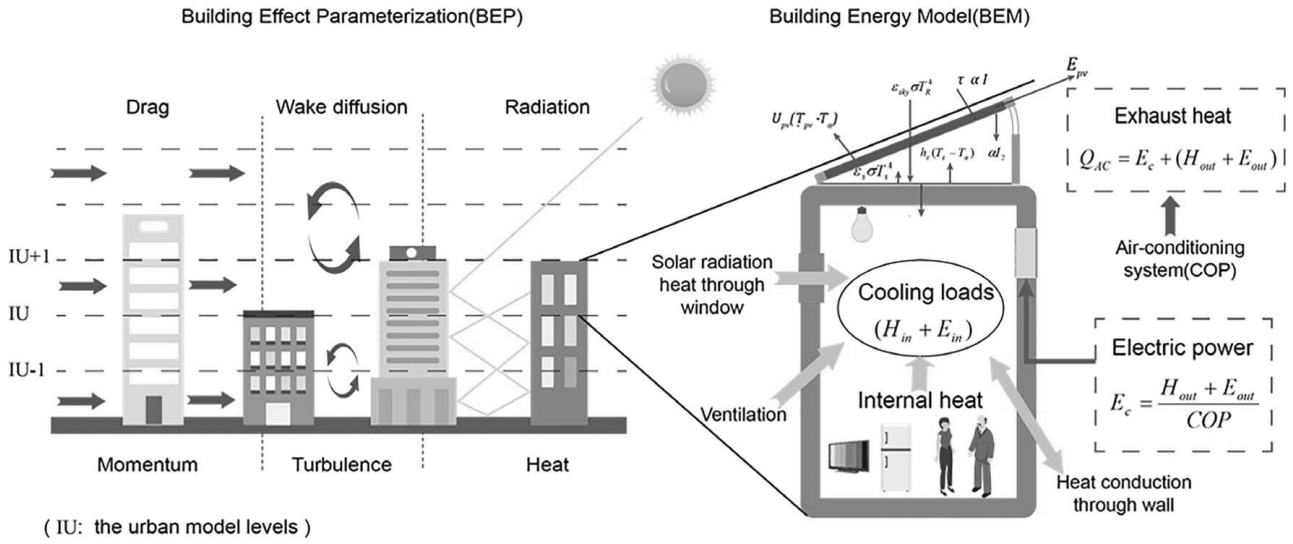

Fig. 2 BEP and modified BEM

$$U_{PV} = 24.1 + 2.9U_a \tag{8}$$

From Eqs. (6)–(8), the surface temperature of PV panel is [46]

$$T_{PV} = \frac{U_{pv}T_a + I[(\tau\alpha)_{PV} - \varepsilon_R - \mu T_{\text{ref}})]}{U_{pv} - \mu I} \tag{9}$$

Surface energy balance over horizontal PV roof

$$(\tau a)_{PV} I = E_{pv} + (h_c + h_r)(T_s - T_a) - k\frac{\mathrm{d}T_s}{\mathrm{d}x} \tag{10}$$

$$T'_s = T_a + \frac{(\tau\alpha)_{PV} I}{h_0} - \frac{E_{pv}}{h_0} \tag{11}$$

Surface energy balance over tilted PV roof

$$a_r I_2 + \varepsilon_{\text{sky}}\sigma T_{R1}^4 - \varepsilon_s \sigma T_s^4 - h_c(T_s - T_a) = -k\frac{\mathrm{d}T_s}{\mathrm{d}x} \tag{12}$$

where I_2 is the radiation from back of the tilted PV panel to roof and is given by

$$I_2 = (h_c + h_r)(T_{PV} - T_a) \tag{13}$$

$$h_r = \varepsilon\sigma(T_s + T_{R1})(T_s^2 + T_{R1}^2) \cong 0.4h_c \text{ when } I_2 > 0$$
$$\cong 0.3h_c \text{ when } I_2 < 0 \tag{14}$$

$$T_{R1} = 1.1T_a - 5 \tag{15}$$

From Eqs. (4), (11)–(15), the surface temperature of tilted PV roof is [44]

$$T'_s = T_a + \frac{a_r I_2}{h_0} - \frac{h_r}{h_0}(5 - 0.1T_a) \tag{16}$$

The final roof temperature for normal roof, horizontal PV roof, and tilted PV roof are calculated using Eq. (17).

$$T_s = T'_s - \frac{U_r}{h_0}(T'_s - T_{\text{ref}}) \tag{17}$$

where U_r is the heat loss coefficient of roof

$$T_{\text{ref}} = 24\,^\circ\text{C}, \quad \varepsilon_R = 15\%\ \mu = 0.07\%\,^\circ\text{C}^{-1}$$

$\alpha_r = 0.85$. For normal roof and 0.3 for cool roof [13] and $\Delta x =$ 17 cm (from original BEP_BEM) [46], $(\tau\alpha)_{PV} = 0.855$, where k is thermal conductivity used from Table 1 for each LCZs.

T_a, U_a, I are used from the WRF outputs.

To quantify the building energy demands on different roof applications, this study employs an urbanized version of WRF model [20], a numerical weather prediction system developed by the National Center for Atmospheric Research. The two urban schemes used in this work are the building effect parameterizations (BEPs) [47] and the building energy model (BEM) [48] that takes into account the shadowing and radiation trapping effects within urban canyons and computes heat fluxes between the indoor and outdoor sides of each buildings accounting the presence of air conditioning systems, windows equipment, and occupancy inside the building's room. It uses indoor heat fluxes based on an hourly schedule to quantify the combination of these components to the building energy budget. The surface temperature of roof in BEP-BEM was modified to incorporate the proposed changes as depicted by Eq. (5) (twice), (11), and (16) to represent normal roof (average albedo of roof 0.15), cool roof (roof albedo 0.7), horizontal PV roof, and tilted PV roof, respectively. Modification of roof surface temperature on BEM due to different roofing application with the energy balance on PV and roof is presented in Fig. 2. To resolve the interaction between the land surface and the atmosphere, the Noah land surface model [49] is used. The Noah land surface model makes use of land use classes to determine thermal, radiative, and hydrological properties of the land surface.

The modified urbanized WRF model is set up to run at a spatial resolution of 1 km by 1 km over the SJMA, where the highest urban density and variability in land cover and land use is found. Two nested domains of decreasing grid spacing (5 km and 1 km) are embedded in areas of interest with a 25 km resolution parent domain as depicted by Fig. 3(*a*). The model was configured to use the rapid radiative transfer modal for longwave radiation [50], the Dudhia scheme for shortwave radiation [51], the Mellor–Yamada–Janjic planetary boundary layer scheme [52], the Kain–Fritsch cumulus parameterization [53], and the WSM6 microphysics [54]. The urban morphology and topography for SJMA are represented by World Urban Database Access Portal Tool (WUDAPT), LCZs as shown in Fig. 3(*b*) previously developed by Pokhrel et al. [13]. Figure 3(*b*) also locates San Juan International Airport (SJIA) and indicates compact high rise (CHR) (1), compact low rise (CLR) (2), and open low rise (OLR) (3) LCZs in the region. It depicts that for SJMA, there is abundant compact low rises with scattered compact high rises, and sparsely built LCZs are dominant more at higher altitudes (altitude is represented

Table 1 Urban parameters used in WRF simulations

Parameters	Units	Compact H rise	Compact M rise	Compact L rise	Open H rise	Open L rise	Large L rise	Sparsely built
Urban fraction	%	100	95	90	65	65	85	30
Roof heat capacity	J/m^3 K	1.95E6	2.4E6	2.219E6	1.95E6	2.219E6	2.4E6	8.916E6
Roof thermal conductivity	W/m K	1.1538	0.937	0.649	1.1538	0.649	0.937	0.1615
Roof albedo	%	13	18	15	13	13	18	13
Roof emissivity	%	91	91	91	91	91	91	91
Roof width	M	15	17.5	9	32	105	28.8	10
Ground heat capacity	J/m^3 K	3.84E6	4.14E6	4.425E6	4.88E6	5.07E6	4.20E6	5.833E6
Ground thermal conductivity	W/m K	0.4004	0.4004	0.4004	0.4004	0.4004	0.4004	0.4004
Ground albedo	%	15	15	16	17	18	16	19
Ground emissivity	%	95	95	95	95	95	95	95
Wall heat capacity	J/m^3 K	1.698E6	4.266E6	3.945E6	2.5E6	3.94E6	2.4E6	15.8E6
Wall thermal conductivity	W/m K	1.1538	0.937	0.649	1.1538	0.649	0.9375	0.1615
Wall albedo	%	25	20	20	25	25	25	25
Wall emissivity	%	90	90	90	90	90	90	90
Road width	m	15	12.7	5.7	37.5	12.4	32.5	10
Building height	m	25	17.5	6.5	25	6.5	6.5	6.5
Building area fraction	%	50	40	40	20	20	20	16
Coefficient of performance of AC system		3	3	3	3	3	3	3
Target temperature of AC system	K	297	297	297	297	297	297	298
Heat generated by equipment	W/m^2	36	30	25	20	15	36	10

by yellow contours). Building heights of Fig. 3(*c*) show a more homogeneous region with heights of 3–10 m with scattered buildings with more than 25 m heights. Initial and boundary conditions used include six-hourly re-analysis with 250 km horizontal resolution, National Center for Environmental Prediction (NCEP-FNL) model for a period of Sep. 29 to Oct. 8, 2014, which represents a high temperature event in between, previously studied by Pokhrel et al. [13,40].

The methodology used in this study involves computing the roof temperature for all roof applications and modify this changes in urban physics (BEP_BEPM) in urban WRF. Heat diffusion equation is solved to compute the temperature in the roof layers in original BEM [21]. However, at the inner most layer and outdoor surface (roof surface), the temperature is defined by solving surface energy budget equation in BEM to compute surface temperatures. Our formulation just changes the roof surface temperature

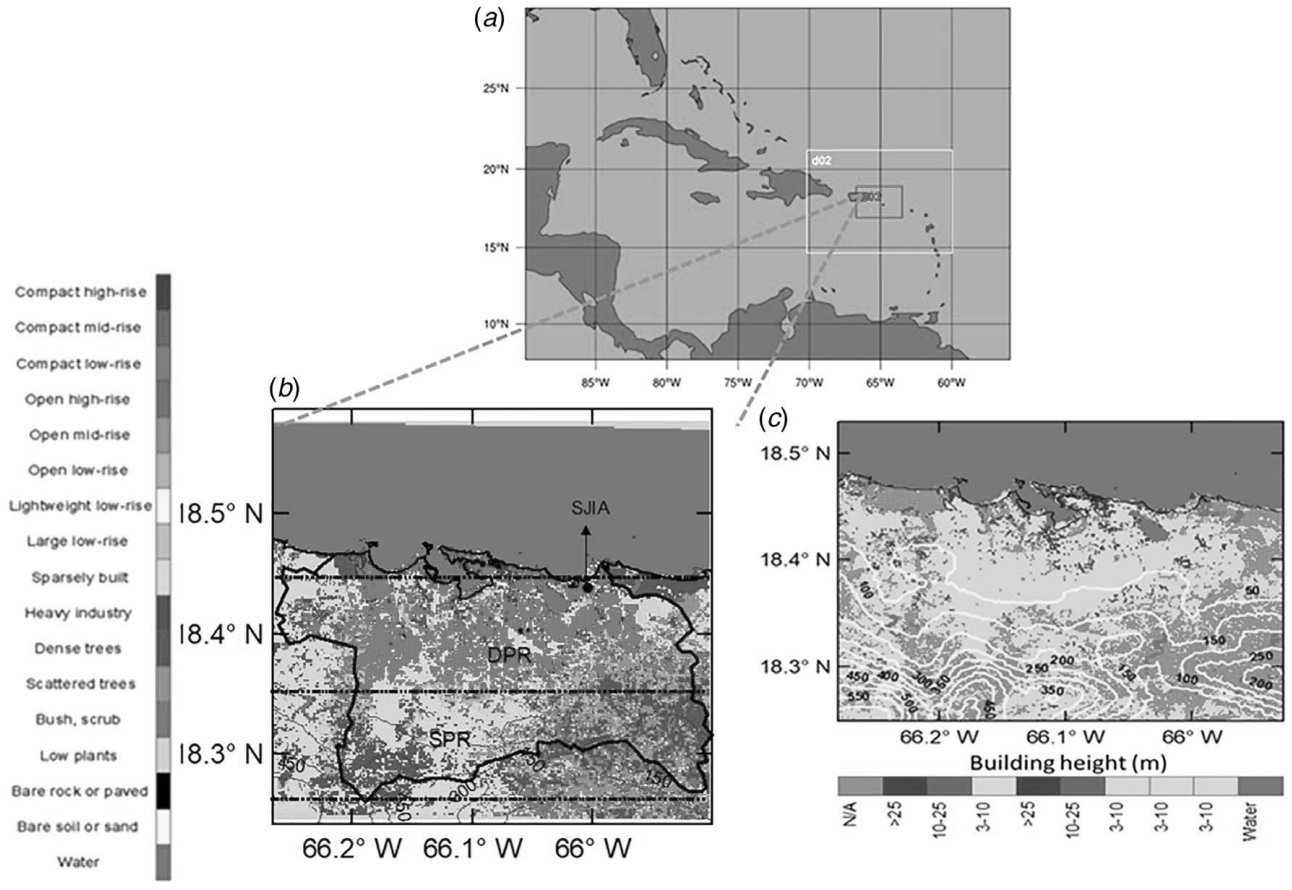

Fig. 3 WRF domain configuration (*a*), WUDAPT LCZs (*b*), and building heights with elevation for SJMA (*c*)

(at outer layer) by solving energy balance equation at the roof surface. The modified version of BEP_BEM utilizes the energy balances over roof surface with empirical correlation for longwave and convective flux with fixed temperature at the interior, i.e., Eqs. (1)–(5) to formulate roof surface temperature. This modification is done in order to evaluate the response to changes in 2 m air temperature and AC demand for PV applications in roof as compared with the normal roof. The effect of different roof applications is studied for temperature and air conditioning demand for SJMA with WUDAPT LCZs. Then, the radiation parameters, output of urban weather research and forecast (uWRF), is further studied to find the power production with PV installation on roof for both horizontal and tilted PV. For this purpose, the isotropic diffuse model, for the direct, diffuse, and ground reflectance components of solar radiation on the tilted and horizontal surface (as shown in Eq. (18)) is used.

$$I = I_b r_b + I_d r_d + (I_b + I_d) r_r \tag{18}$$

Equation (18) is used with Eq. (7) to give the PV power output both for a horizontal surface and a tilted surface of 20 deg. Where I is the radiation on a tilted and horizontal surface, I_b is direct, and I_d is the diffuse radiation. The radiation components of the beam (direct), diffuse, and ground reflectance is given in Eq. (19)

$$r_b = \frac{\sin\delta \sin(\phi - \beta) + \cos\,\delta\, \cos(\phi - \beta) \cos\,\omega}{\sin\delta\, \sin\,\phi + \cos\,\delta\, \cos\,\phi\, \cos\,\omega}$$
$$r_d = \frac{1 + \cos\,\beta}{2} \quad r_r = \frac{1 - \cos\,\beta}{2} \tag{19}$$

The different urban parameters used in the WRF simulations are presented in Table 1.

3 Results

3.1 Model Validation. The offline version of roof temperature (T_s) is presented for different roof applications, namely, NR, horizontal PV roof (HPV), tilted PV roof (TPV), and cool roof (CR) as shown in Fig. 4 with an input from urban WRF variables. The roof temperature is seen to be maximum for NR and HPV reaching as high as 50 °C, whereas for tilted PV roof and cool roof the maximum temperature reduces by 8–13 °C, respectively. The minimum temperature however is the same for normal roof and cool roof, whereas it is higher by 2–3 deg for HPV roof. The maximum roof temperature for NR, HPV roof, and TPV roof is also measured to be 60 °C, 58 °C, and 42 °C for a hot summer day in the city of San Diego, CA [34]. In another study, on the similar day in the city of Chicago, the maximum roof temperature for cool roof was measured to be 40 °C [55], consistent with our results. The results of modified version of BEP_BEM for 2 m air temperature for different roof application including the original version of BEP_BEM (without modification) is compared with the observation from SJIA in Fig. 4(*b*). To validate the simulated temperature (estimator) with the observation (SJIA), linear regression was applied both for modified BEP_BEM and original BEP_BEM including the residuals. Both models appear to fit the data well and the residuals appear to be randomly distributed around zero indicating that the models describe the data well. Therefore, the graphical evaluation of the fits (of Fig. 4) does not reveal any obvious differences between the two models. However, the fits and residuals fail to capture the slight overestimation of 2 m air temperatures for some days for modified roof surface temperature of BEP_BEM and are attributed to low wind speeds during these days. For the purpose of this study, that is to evaluate the response of PV applications of roof on 2 m air temperature and AC demand difference, this assumption (changes in roof surface temperature due to PV installation) is followed in all configurations in order to create a consistency in the formulations. In previous studies,

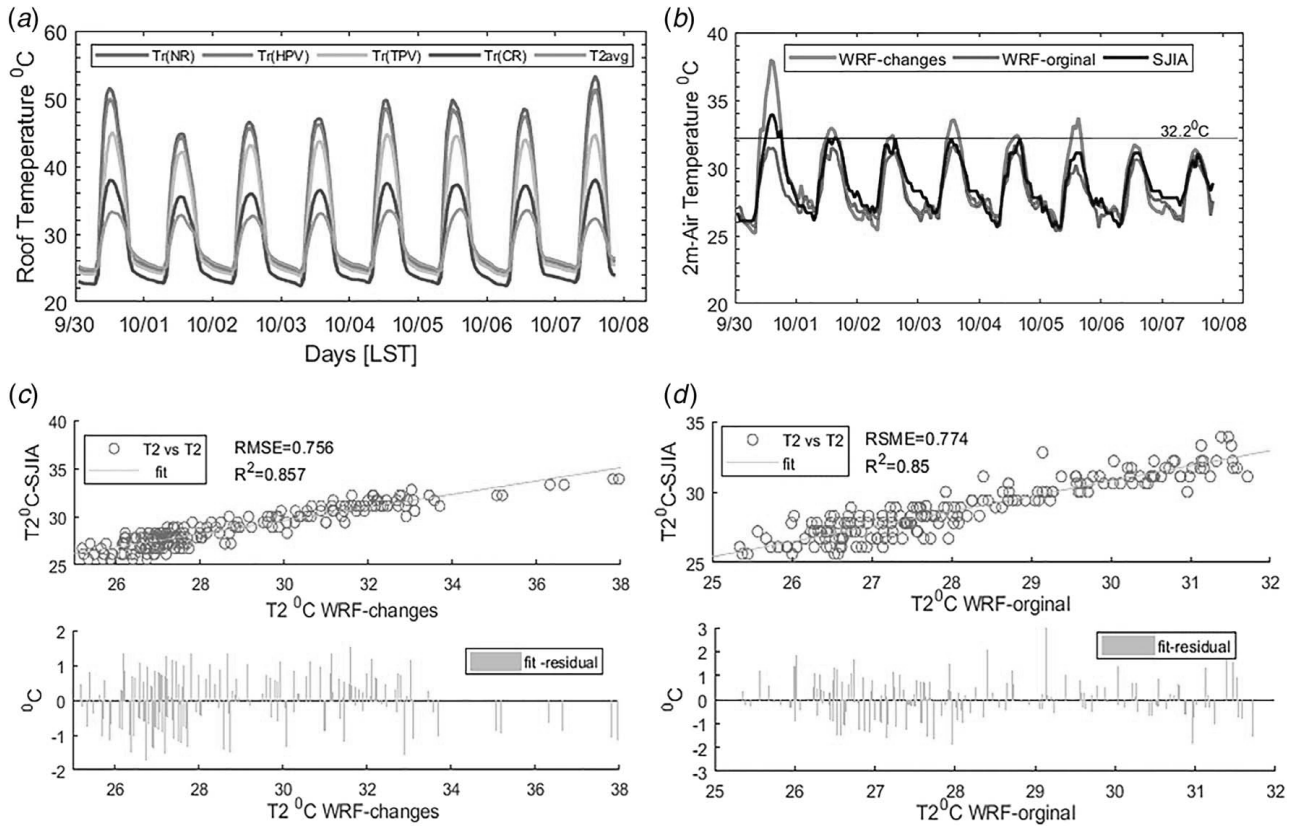

Fig. 4 Roof temperatures and 2 m air temperature (*a*), modified urban WRF and SJIA and original WRF, 2 m-air temperature (*b*), linear fit of modified WRF 2 m air temperature and SJIA temperature with its residuals (c), and linear fit of original WRF 2 m air temperature and SJIA temperature with its residuals (*d*)

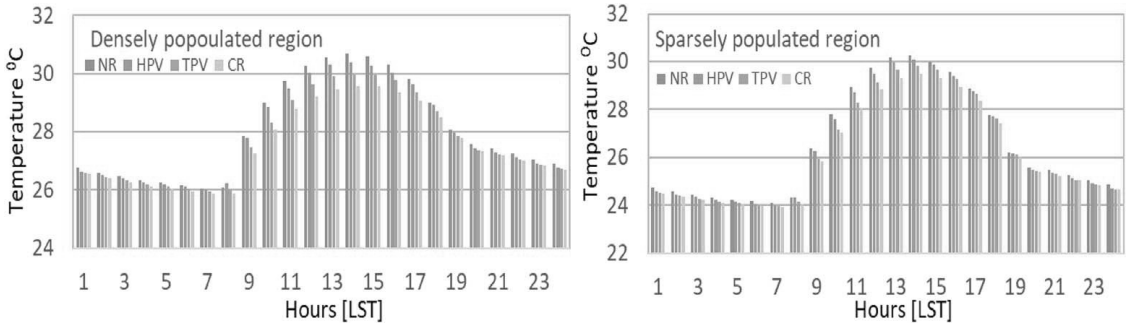

Fig. 5 Average 2-m air temperature for densely and sparsely populated region for Sep. 29 to Oct. 8, 2014

temperature, humidity, wind speed, wind direction, and potential temperature have been validated for the same input data. In addition to the metrological variables, the air conditioning demand from urban WRF have also been compared with the utility records and validated with Energy Plus™ software [13]. The global horizontal irradiance of WRF for dense urban settings of New York has recently been validated with the observational records for clear, cloudy, and overcast conditions [56]. We use the similar approach to compute total radiation on horizontal and tilted surfaces.

3.2 Temperatures and Urban Heat Island. The UHI for San Juan, Puerto Rico is studied to increase at a rate of 0.06 °C per year and estimated to reach as high as 8 °C by 2050 [42]. In order to understand the role of roof applications on UHI, a time series of 2-m air temperature for densely populated and sparsely populated region (as delineated in Fig. 2(*b*)) is presented in Fig. 5 along with spatial plots of maximum and minimum temperatures as represented in Fig. 6. For densely populated region, the maximum temperature is simulated to be higher than 30 °C for NR and HPV roof but less than 30 °C for sparsely populated region. The minimum temperature for densely populated region is higher by 2 °C compared with the sparsely populated region. Also, the minimum temperature for densely populated region for HPV roof is simulated to be 0.25 deg higher than NR during 8 a.m. LST. In other words, HPV slightly reduces the daytime UHI, whereas it increases the peak night time UHI. NR, HPV, TPV, and CR show maximum 2 m air temperature in the decreasing order, where TPV reduces it

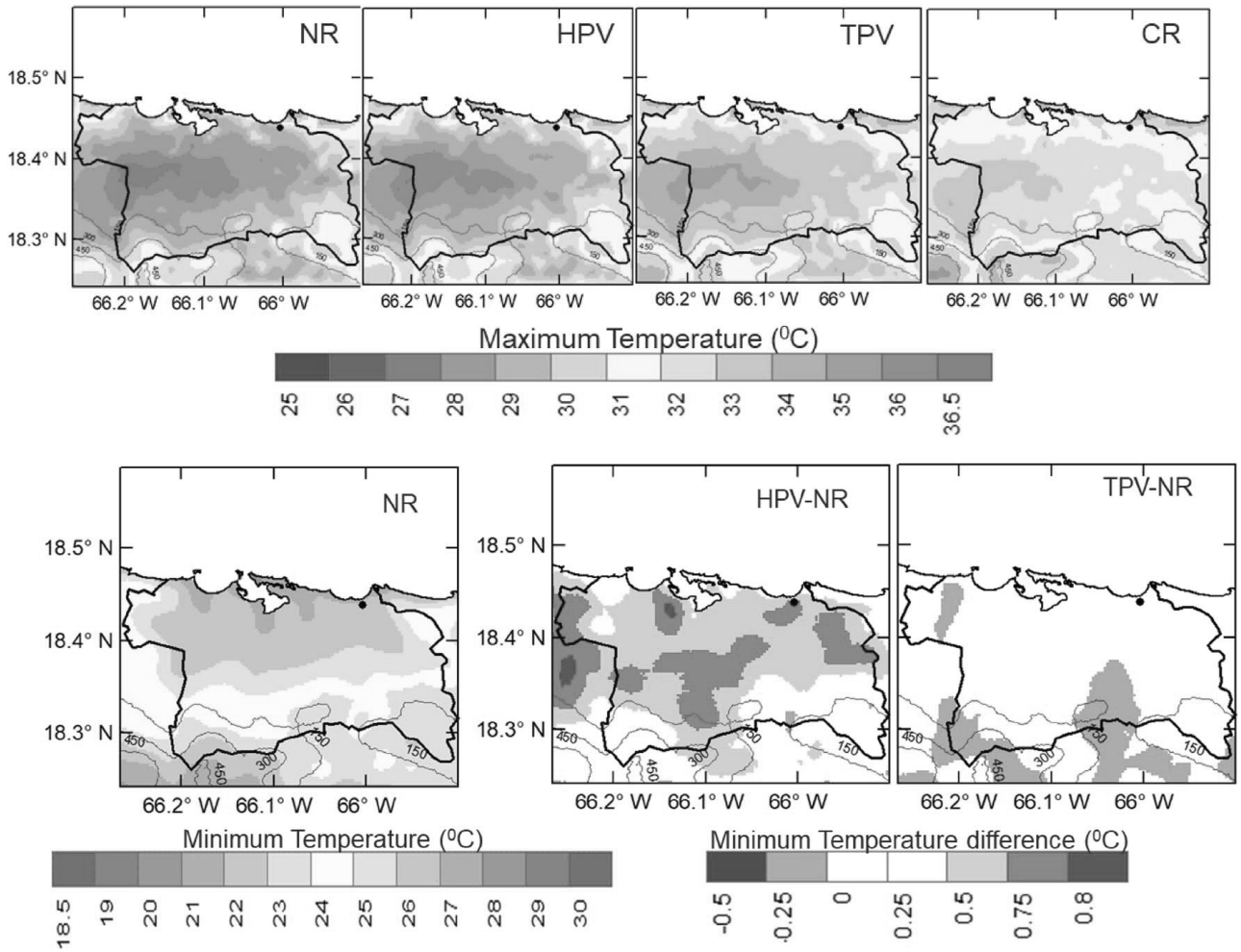

Fig. 6 2 m-maximum temperature (14 LST) for NR, HPV, TPV, and CR, 2 m minimum temperature (6LST) for NR and the minimum temperature difference for HPV-NR and TPV-NR

Table 2 AC demand per day for different LCZs and roof applications

	AC demand GW h/day			
LCZ/roofs	NR	HPV	TPV	CR
LCZ1	3.08	3.01	2.92	2.81
LCZ2	1.2	1	0.94	0.89
LCZ3	17.22	18.17	16.79	15.14
LCZ4	0.142	0.135	0.13	0.126
LCZ6	1.41	1.44	1.3	1.165
LCZ8	0.09	0.09	0.08	0.073
LCZ9	0.68	0.72	0.675	0.62
Total	23.822	24.565	22.835	20.824

by 2 °C and CR reduces it by 4–5 °C at compact low rise LCZs compared with NR. The minimum temperature, however, for NR is 26 °C, whereas the difference of minimum temperature for HPV with NR indicates an increase in UHI by 0.5–0.75 °C. The increase in night time UHI for HPV is due to the absence of radiative cooling from HPV roof as compared with NR. There are, however, no significant changes in night time UHI for TPV and CR.

3.3 Impacts on Air Conditioning Demand. The average total air conditioning demand for each LCZ on a day for the entire SJMA is shown in Table 2, for different roof applications. The W/m^2 is per horizontal grids and includes both built and non-built surfaces. However, the sum of AC demand for each LCZs is multiplied by building area fraction in order to compute the total AC demand of Table 2, which has been previously used by Pokhrel et al. [13]. Compact high rise and compact low rise together represents more than 85% of the total air conditioning demand for the region. TPV and CR decreases the total demand by 4% and 12%, respectively; however, HPV roof increases the demand by 3%. The increase in AC demand for HPV roof is attributed to net increase in UHI during night and morning hours. The peak AC demand for normal roof follows the LCZs distribution, height of 20 W/m^2 at compact high rise, 10–12 W/m^2 at compact low rise, and 6–8 W/m^2 at open low rise as presented in Fig. 7. In previous studies [13], the total AC demand for the same time period is compared with the utility data and it was found to be very comparable with this study. We are collaborating with the Puerto Rico Power Authority to share hourly data of electrical energy demand, which will allow us to extract the AC hourly demand using well-known methods for baseline loads [57].

Peak AC demand savings of 0.5–1 W/m^2 is simulated for the TPV and 1.5–2 W/m^2 for CR, respectively, for compact low rise LCZ. The peak demand savings potential for tilted PV and CR for some location in the metropolitan area is equivalent to 8% and 16%, respectively. However, the peak demand reduction potential for HPV roof is very insignificant and is not presented in Fig. 7.

3.4 Photovoltaic Power Potential. Radiation components are the important parameters in estimating the PV power potential. The output from urban WRF for shortwave direct normal (SWDDNI), shortwave direct diffuse (SWDDIF), downward shortwave (SWDOWN), and total radiation (as estimated utilizing Eqs. (17) and (18) on tilted surface of 20 deg (Total I) is presented in Fig. 8. For the entire simulation period, large cloud cover is

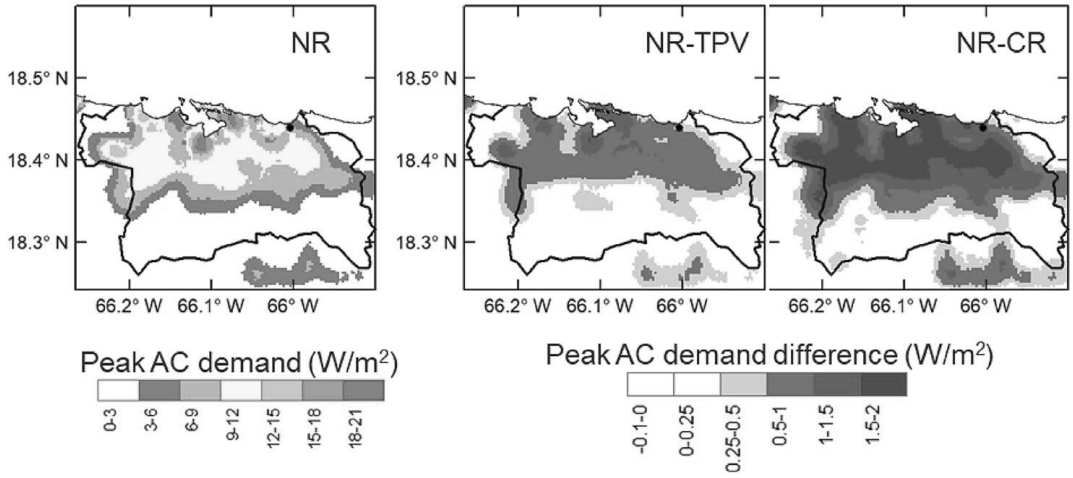

Fig. 7 Peak AC demand (normal roof) and peak AC demand savings for normal roof-tilted PV roof and normal roof-cool roof

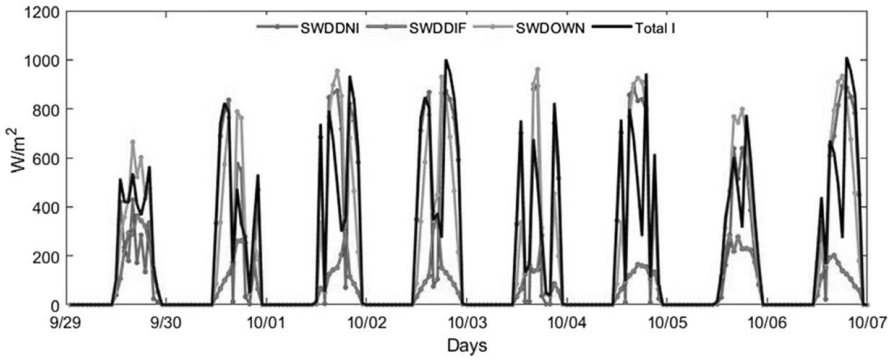

Fig. 8 Radiation components for grid point closest to SJIA

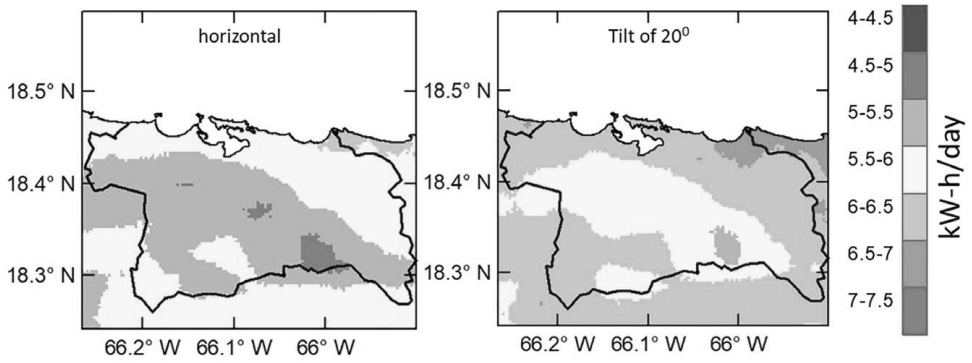

Fig. 9 Spatial profile of daily solar total radiation on a horizontal and tilted surface for SJMA

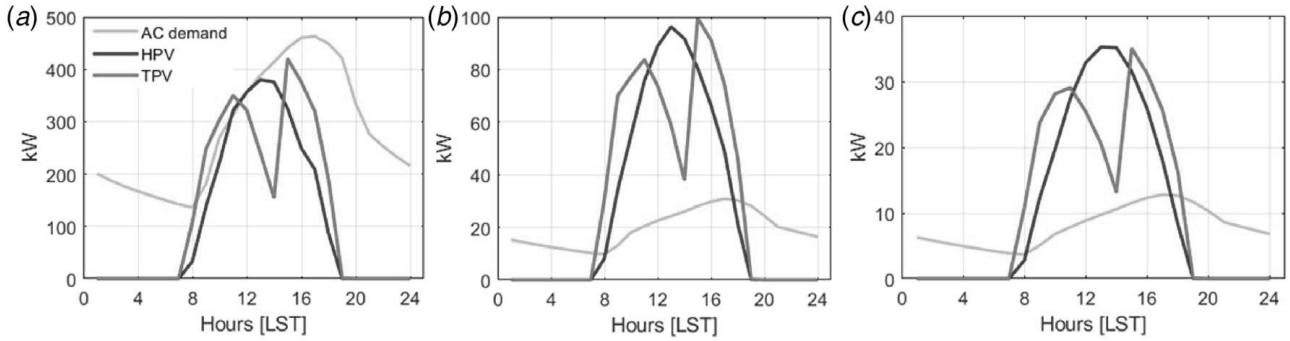

Fig. 10 Hourly average AC demand and PV power from horizontal PV and titled PV for large hotel (*a*), multifamily low rise apartment (*b*), and single family detached unit (c). For the entire simulation period of Sep. 30, 2014, to Oct. 7, 2014.

simulated during late morning and midafternoon hours. However, for tilted surface, early morning and late afternoon hours are simulated to have more incoming radiation than the horizontal surface.

Daily solar total radiation on a titled surface of 20 deg is 8.7% more than the daily solar radiation on a horizontal surface for SJMA for a day on the month of October as shown in Fig. 9. The values of daily solar total radiation are comparable with those estimated by open source tools such as PV Watts,[5] which estimates average daily solar radiation for SJMA for the month of October for horizontal and 20 deg tilted surface to be equal to 5.25–5.88 kW h/day, respectively. However, the modeled results are 5.75 and 6.25 kW h/day with an overestimation of 0.5 and 0.37 kW h/day for both horizontal and tilted surfaces, respectively.

Hourly average AC demand and PV power production for large office represented as CHR, multifamily low rise apartment represented as CLR, and single family detached unit represented as OLR for both HPV and TPV is shown in Fig. 10. The floor areas for large office (CHR), multifamily low rise apartment (CLR), and single family detached (OLR) unit are 41,549 ft^2 (3860 m^2), 10,404 ft^2 (967 m^2), and 3602 ft^2 (335 m^2) taken from US DOE reference buildings.[6] For large office (Fig. 10(*a*)), hourly demand peaks at 463 kW with daily AC demand reaches 6790 kW h/day whereas productions are 2670 and 3032 kW h/day for horizontal and tilted PV, respectively. For multifamily (Fig. 10(*b*)), the hourly demand peaks at 31 kW with the daily demand as 467 kW h/day, whereas production is 667 and 744 kW h for HPV and TPV, respectively. Demand and production for single family detached unit (Fig. 10(*c*)) are 190, 250, and 260 kW h, respectively, with a peak demand of 13 kW.

Figure 11 presents weekly AC demand for normal roof, HPV roof, and TPV roof and available roof area for each LCZs in the region of interest consisting entire SJMA. It is simulated that for high rise and midrise, the demand is close to power production given the small total roof area. However, for CLR and OLR, the AC demand is 20–22% of the power production potential, indicating that 22% of the suitable roof area is enough to meet the total AC demands for the CLR and OLR LCZs.

4 Conclusions and Future Studies

Our goal in this study is to investigate environmental and energy sustainability of an urban coastal tropical city utilizing different building integrated roofing technologies. Tropical coastal cities are experiencing rapid energy growth due to economic development and a rapid changing climate. This study utilizes the changes in roof surface for normal roof, horizontal PV roof, tilted PV roof, and cool roof to investigate 2-m air and roof temperatures along with AC energy demands. The radiation parameters are further utilized to

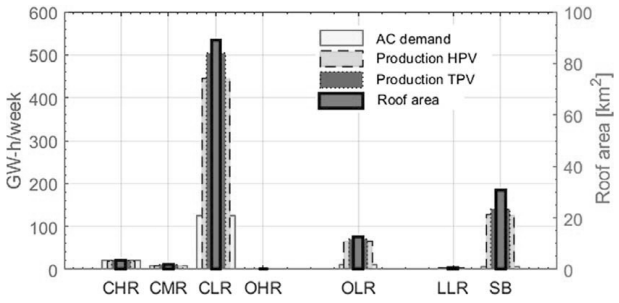

Fig. 11 Weekly AC demand in GW h, weekly power output from horizontal PV and tilted PV in GW h with available roof area for total CHR, compact midrise (CMR), CLR, OLR, large low rise (LLR), and sparsely built (SB) LCZs

[5]https://pvwatts.nrel.gov/
[6]https://www.energy.gov/eere/buildings/commercial-reference-buildings

study the PV power potential. A new methodology is presented that represents the integration of solar PV technologies in buildings and scale up to the whole city. The WUDAPT LCZs for the SJMA is represented mostly by compact low rises, sparsely built and open low rises with scattered areas of compact high rises. The case study of the city of San Juan, Puerto Rico is considered due to the potential of this city to undergo rapid changes as part of the energy transformation post Hurricane Maria. The peak roof temperature is seen to be maximum for NR and HPV reaching higher than 54 °C, whereas for tilted PV roof and cool roof the maximum temperature reduces to 46 and 41 °C, respectively. As a result, the reduction in peak AC demand is simulated to be 8% for tilted PV roof and 16% for cool roof for some locations in SJMA. Horizontal PV does not show significant changes in peak AC demand compared with normal roof; however, the daily demand for HPV is seen to increase by 3% and decrease by 4% and 10% for TPV and CR, respectively. For the month of October 2014, the daily total radiation on a tilted surface is 5.5–6.5 kWh/m^2 for SJMA, which is 6–10% higher than daily total radiation on a horizontal surface. Finally, the ratio of AC demand to PV power production for compact high rise and compact midrise LCZs is close to 1; however, for compact low rise and open low rise, it is 0.2. The proposed methodology of PV power potential and cooling load mitigation alternatives may have similar results in other tropical coastal cities, although the magnitude would be different depending on the size, form, and function of the urban coverage. Future studies will be focused on utilizing both active and passive building integrated technologies for mitigating heat during extreme conditions for different climate change scenarios.

Nomenclature

I = total solar radiation
a_r = abrobtivity of roof
h_c = convective heat transfer coefficient
h_r = radiative heat transfer coefficient
E_{pv} = PV power production
I_b = beam or direct radiation
I_d = diffuse radiation
T_a = ambient temperature
T_{room} = room temperature
T_{ref} = reference temperature
T_s = surface temperature
T_{PV} = temperature of PV panel
T_R = radiant temperature of horizontal surface
T_{Rl} = radiant temperature of tilted surface
U_a = wind speed
U_{pv} = PV loss coefficient
U_r = heat loss coefficient of roof
T_s' = sol–air temperature
β = tilt
δ = declination
Δx = roof thickness
ε_s = emissivity of surface
ε_{sky} = emissivity of sky
ε_R = reference module efficiency
μ = temperature coefficient
σ = Stefan Boltzmann constant
$\tau\alpha_{PV}$ = transmitivity of glass and absorptivity of PV panel
ϕ = latitude
ω = hour angle

Acronym

LCZs = local climate zones

Acknowledgment

The authors would like to acknowledge the assistance and suggestions from the members of the Coastal Urban Environmental Research Group from City College New York and of the University of Puerto Rico Mayaguez. The analysis process was conducted at the high performance computing facilities at City College of New York (http://cuerg.ccny.cuny.edu/) and College of Staten Island CUNY, high performance computing center (https://cunyhpc.csi.cuny.edu/). Financial support for this research was provided by the US National Science Foundation (Grant No. CBET-1438324; Funder ID: 10.13039/100000001) and the US Agency for International Development (Grant No. AID-517-A-15-00002; Funder ID: 10.13039/100000200).

References

[1] Kumar Sahu, B., 2015, "A Study on Global Solar PV Energy Developments and Policies With Special Focus on the Top Ten Solar PV Power Producing Countries," Renew. Sustain. Energy Rev., **43**, pp. 621–634.
[2] Stoeglehner, G., Niemetz, N., and Kettl, K. H., 2011, "Spatial Dimensions of Sustainable Energy Systems: New Visions for Integrated Spatial and Energy Planning," Energy Sustain. Soc., **1**(1), pp. 1–9.
[3] Wang, N., Phelan, P. E., Gonzalez, J., Harris, C., Henze, G. P., Hutchinson, R., Langevin, J., Lazarus, M. A., Nelson, B., Pyke, C., Roth, K., Rouse, D., Sawyer, K., and Selkowitz, S., 2017, "Ten Questions Concerning Future Buildings Beyond Zero Energy and Carbon Neutrality," Build. Environ., **119**, pp. 169–182.
[4] Wittmann, H., Bajons, P., Doneus, M., and Friesinger, H., 1997, "Identification of Roof Areas Suited for Solar Energy Conversion Systems," Renew. Energy, **11**(1), pp. 25–36.
[5] Izquierdo, S., Rodrigues, M., and Fueyo, N., 2008, "A Method for Estimating the Geographical Distribution of the Available Roof Surface Area for Large-Scale Photovoltaic Energy-Potential Evaluations," Sol. Energy, **82**(10), pp. 929–939.
[6] Hofierka, J., and Kaňuk, J., 2009, "Assessment of Photovoltaic Potential in Urban Areas Using Open-Source Solar Radiation Tools," Renew. Energy, **34**(10), pp. 2206–2214.
[7] Strzalka, A., Alam, N., Duminil, E., Coors, V., and Eicker, U., 2012, "Large Scale Integration of Photovoltaics in Cities," Appl. Energy, **93**, pp. 413–421.
[8] Hong, T., Lee, M., Koo, C., Jeong, K., and Kim, J., 2017, "Development of a Method for Estimating the Rooftop Solar Photovoltaic (PV) Potential by Analyzing the Available Rooftop Area Using Hillshade Analysis," Appl. Energy, **194**, pp. 320–332.
[9] Office of Energy Efficiency & Renewable Energy (EERE), and U.S. Department of Energy, 2012, "2011 Buildings Energy Data Book," US DOE, pp. 1–81.
[10] Ürge-Vorsatz, D., Cabeza, L. F., Serrano, S., Barreneche, C., and Petrichenko, K., 2015, "Heating and Cooling Energy Trends and Drivers in Buildings," Renew. Sustain. Energy Rev., **41**, pp. 85–98.
[11] Crawley, D. B., 2008, "Estimating the Impacts of Climate Change and Urbanization on Building Performance," J. Build. Perform. Simul., **1**(2), pp. 91–115.
[12] Lu, N., et al., 2009, "Climate Change Impacts on Residential and Commercial Loads in the Western U.S. Grid," IEEE Trans. Power Syst., **25**(1), pp. 480–488.
[13] Pokhrel, R., Ramírez-Beltran, N. D., and González, J. E., 2019, "On the Assessment of Alternatives for Building Cooling Load Reductions for a Tropical Coastal City," Energy Build., **182**, pp. 131–143.
[14] Ramirez-Beltran, N. D., Gonzalez, J. E., Castro, J. M., Angeles, M., Harmsen, E. W., and Salazar, C. M., 2017, "Analysis of the Heat Index in the Mesoamerica and Caribbean Region," J. Appl. Meteorol. Climatol., **56**(11), pp. 2905–2925.
[15] Angeles-malaspina, M., González-cruz, J. E., and Ramírez-beltran, N., 2018, "Projections of Heat Waves Events in the Intra-Americas Region Using Multimodel Ensemble," Adv. Meteorol., **2018**, pp. 18–21.
[16] Méndez-Lázaro, P. A., Pérez-Cardona, C. M., Rodríguez, E., Martínez, O., Taboas, M., Bocanegra, A., and Méndez-Tejeda, R., 2018, "Climate Change, Heat, and Mortality in the Tropical Urban Area of San Juan, Puerto Rico," Int. J. Biometeorol., **62**(5), pp. 699–707.
[17] J. E. González, M. Georgescu, M. C. Lemos, N. Hosannah, and D. Niyogi, "Climate Change's Pulse is in Central America and the Caribbean," EOS, 98. Published on Apr. 27, 2017.
[18] Rekinger,, M, Thies,, F, and SolarPower Europe, 2019, "Global Market Outlook for Solar Power 2015–2019," SolarPower Europe. www.solarpowereurope.org
[19] J. M. H. Villamar and J. A. Diaz, "Co-operative Programme on Photovoltaic National Survey Report of PV Power Applications in Mexico," May, 2011.
[20] Skamarock, W. C., Klemp, J. B., Dudhia, J., Gill, D. O., Barker, D. M., Wang, W., and Powers, J. G., 2008, "A Description of the Advanced Research WRF Version 3," Tech. Rep., June, p. 113.
[21] Salamanca, F., Krpo, A., Martilli, A., and Clappier, A., 2010, "A new Building Energy Model Coupled With an Urban Canopy Parameterization for Urban Climate Simulations-Part I. Formulation, Verification, and Sensitivity Analysis of the Model," Theor. Appl. Climatol., **99**(3–4), pp. 331–344.
[22] Salamanca, F., Georgescu, M., Mahalov, A., Moustaoui, M., and Martilli, A., 2016, "Citywide Impacts of Cool Roof and Rooftop Solar Photovoltaic Deployment on Near-Surface Air Temperature and Cooling Energy Demand," Boundary Layer Meteorol., **161**(1), pp. 203–221.
[23] Masson, V., Bonhomme, M., Salagnac, J.-L., Briottet, X., and Lemonsu, A., 2014, "Solar Panels Reduce Both Global Warming and Urban Heat Island," Front. Environ. Sci., **2**, p. 14.

[24] Roman, K. K., O'Brien, T., Alvey, J. B., and Woo, O. J., 2016, "Simulating the Effects of Cool Roof and PCM (Phase Change Materials) Based Roof to Mitigate UHI (Urban Heat Island) in Prominent US Cities," Energy, **96**, pp. 103–117.
[25] Akbari, H., Pomerantz, M., and Taha, H., 2001, "Cool Surfaces and Shade Trees to Reduce Energy Use and Improve Air Quality in Urban Areas," Sol. Energy, **70**(3), pp. 295–310.
[26] Oleson, K. W., Bonan, G. B., and Feddema, J., 2010, "Effects of White Roofs on Urban Temperature in a Global Climate Model," Geophys. Res. Lett., **37**(3), p. L03701.
[27] Cotana, F., Rossi, F., Filipponi, M., Coccia, V., Pisello, A. L., Bonamente, E., Petrozzi, A., and Cavalaglio, G., 2014, "Albedo Control as an Effective Strategy to Tackle Global Warming: A Case Study," Appl. Energy, **130**, pp. 641–647.
[28] Ortiz, L. E., Gonzalez, J. E., Gutierrez, E., and Arend, M., 2016, "Forecasting Building Energy Demands With a Coupled Weather-Building Energy Model in a Dense Urban Environment," ASME J. Sol. Energy Eng., **139**(1), p. 011002.
[29] Sharma, A., Conry, P., Fernando, H. J. S., Hamlet, A. F., Hellmann, J. J., and Chen, F., 2016, "Green and Cool Roofs to Mitigate Urban Heat Island Effects in the Chicago Metropolitan Area: Evaluation With a Regional Climate Model," Environ. Res. Lett., **11**(6), p. 064004.
[30] Comarazamy, D. E., González, J. E., and Luvall, J. C., 2015, "Quantification and Mitigation of Long-Term Impacts of Urbanization and Climate Change in the Tropical Coastal City of San Juan, Puerto Rico," Int. J. Low-Carbon Technol., **10**(1), pp. 87–97.
[31] Vázquez Morales, W., Jazcilevich, A., García Reynoso, A., Caetano, E., Gómez, G., and Bornstein, R. D., 2016, "Influence of Green Roofs on Early Morning Mixing Layer Depths in Mexico City," ASME J. Sol. Energy Eng., **138**(6), p. 061011.
[32] Barron-Gafford, G. A., Minor, R. L., Allen, N. A., Cronin, A. D., Brooks, A. E., and Pavao-Zuckerman, M. A., 2016, "The Photovoltaic Heat Island Effect: Larger Solar Power Plants Increase Local Temperatures," Sci. Rep., **6**, pp. 1–7.
[33] Lebassi, B., González, J. E., and Bornstein, R. D., 2013, "On the Environmental Sustainability of Building Integrated Solar Technologies in a Coastal City," ASME J. Sol. Energy Eng., **135**(4), p. 040904.
[34] Dominguez, A., Kleissl, J., and Luvall, J. C., 2011, "Effects of Solar Photovoltaic Panels on Roof Heat Transfer," Sol. Energy, **85**(9), pp. 2244–2255.
[35] Poupkou, A., Nastos, P., Melas, D., and Zerefos, C., 2011, "Climatology of Discomfort Index and Air Quality Index in a Large Urban Mediterranean Agglomeration," Water Air Soil Pollut., **222**(1–4), pp. 163–183.
[36] Lai, L.-W., and Wan-Li, C., 2010, "Urban Heat Island and Air Pollution—An Emerging Role for Hospital Respiratory Admissions in an Urban Area," J. Environ. Health, **72**(6), pp. 32–35.
[37] McGregor, G. R., Markou, M. T., Bartzokas, A., and Katsoulis, B. D., 2002, "An Evaluation of the Nature and Timing of Summer Human Thermal Discomfort in Athens, Greece," Clim. Res., **20**(1), pp. 83–94.
[38] Pantavou, K., Theoharatos, G., Nikolopoulos, G., Katavoutas, G., and Asimakopoulos, D., 2008, "Evaluation of Thermal Discomfort in Athens Territory and its Effect on the Daily Number of Recorded Patients at Hospitals' Emergency Rooms," Int. J. Biometeorol., **52**(8), pp. 773–778.
[39] Lemonsu, A., Viguié, V., Daniel, M., and Masson, V., 2015, "Vulnerability to Heat Waves: Impact of Urban Expansion Scenarios on Urban Heat Island and Heat Stress in Paris (France)," Urban Clim., **14**(Part 4), pp. 586–605.
[40] Pokhrel, R., Ortiz, L. E., Ramírez-Beltran, N. D., and González, J. E., 2018, "On the Climate Variability and Energy Demands for Indoor Human Comfort Levels in a Tropical-Coastal Urban Environment," ASME J. Sol. Energy Eng., **141**(3), p. 031002.
[41] Comarazamy, D. E., González, J. E., Luvall, J. C., Rickman, D. L., and Bornstein, R. D., 2013, "Climate Impacts of Land-Cover and Land-Use Changes in Tropical Islands Under Conditions of Global Climate Change," J. Clim., **26**(5), pp. 1535–1550.
[42] Velazquez-Lozada, A., Gonzalez, J. E., Winter, A., and Mulero, P. J., "Urban Heat Island Studies for San Juan, Puerto Rico," J. Atmos. Environ., **40**(9), pp. 1731–1741.
[43] Bureau, E., Rico, P., and Power, E., 2019, "Puerto Rico Integrated Resource Plan Draft for the Review of the Puerto Rico Energy Bureau Prepared for Puerto Rico Electric Power Authority," Integrated Resource Plan, **1**(518).
[44] Höglund, B. I., Mitalas, G. P., and Stephenson, D. G., 1967, "Surface Temperatures and Heat Fluxes for Flat Roofs," Build. Sci., **2**(1), pp. 29–36.
[45] Defraeye, T., Blocken, B., and Carmeliet, J., 2011, "Convective Heat Transfer Coefficients for Exterior Building Surfaces: Existing Correlations and CFD Modelling," Energy Convers. Manage., **52**(1), pp. 512–522.
[46] Mattei, M., Notton, G., Cristofari, C., Muselli, M., and Poggi, P., 2006, "Calculation of the Polycrystalline PV Module Temperature Using a Simple Method of Energy Balance," Renew. Energy, **31**(4), pp. 553–567.
[47] Martilli, A., Clappier, A., and Rotach, M. W., 2002, "An Urban Surface Exchange Parameterisation for Mesoscale Models," Boundary Layer Meteorol., **104**(2), pp. 261–304.
[48] Salamanca, F., and Martilli, A., 2010, "A New Building Energy Model Coupled With an Urban Canopy Parameterization for Urban Climate Simulations-Part II. Validation With One Dimension Off-Line Simulations," Theor. Appl. Climatol., **99**(3–4), pp. 345–356.
[49] Tewari, M., Chen, F., Wang, W., Dudhia, J., LeMone, M., Mitchell, K., Ek, M., Gayno, G., Wegiel, J., and Cuenca, R., 2004, "Implementation and Verification of the Unified NOAH Land Surface Model in the WRF Model," 20th Conference on Weather Analysis and Forecasting/16th Conference on Numerical Weather Prediction, Seattle, WA, Jan. 10–15, pp. 11–15.
[50] Mlawer, E. J., Taubman, S. J., Brown, P. D., Iacono, M. J., and Clough, S. A., 1997, "Radiative Transfer for Inhomogeneous Atmospheres: RRTM, a Validated Correlated-k Model for the Longwave," J. Geophys. Res. Atmos., **102**(D14), pp. 16663–16682.
[51] Dudhia, J., 1989, "Numerical Study of Convection Observed During the Winter Monsoon Experiment Using a Mesoscale Two-Dimensional Model," J. Atmos. Sci., **46**(20), pp. 3077–3107.
[52] Janjić, Z. I., 1994, "The Step-Mountain Eta Coordinate Model: Further Developments of the Convection, Viscous Sublayer, and Turbulence Closure Schemes," Mon. Weather Rev., **122**(5), pp. 927–945.
[53] Kain, J. S., 2004, "The Kain–Fritsch Convective Parameterization: An Update," J. Appl. Meteorol., **43**(1), pp. 170–181.
[54] Hong, S., and Lim, J., 2006, "The WRF Single-Moment 6-Class Microphysics Scheme (WSM6)," J. Korean Meteorol. Soc., **42**(2), pp. 129–151.
[55] Scherba, A., Sailor, D. J., Rosenstiel, T. N., and Wamser, C. C., 2011, "Modeling Impacts of Roof Reflectivity, Integrated Photovoltaic Panels and Green Roof Systems on Sensible Heat Flux Into the Urban Environment," Build. Environ., **46**(12), pp. 2542–2551.
[56] Gamarro, H., Gonzalez, J., and Ortiz, L., 2019, "Evaluation of Urban WRF-Solar for PV Power Forecasts in Cities," J. Energy Resour. Technol., **141**, pp. 1–7.
[57] Ortiz, L. E., Gonzalez, J. E., and Lin, W., 2018, "Climate Change Impacts on Peak Building Cooling Energy Demand in a Coastal Megacity," Environ. Res. Lett., **13**(9), p. 094008.